

Article

Influence of the Nano-Iron Oxide Adsorption-Enhanced Microstructured Charcoal Additives on the ANFO's Properties

Andrzej Biessikirski ^{1,*}, Suzana Gotovac Atlagić ², Mateusz Pytlik ³, Łukasz Kuterasiński ⁴, Michał Dworzak ¹, Michał Twardosz ¹, Marek Cała ¹, Joanna Jakóbczyk ¹, Sunčica Sukur ², Agnieszka Stopkowicz ¹, Andrzej Baziak ⁵ and Bogna Daria Napruszewska ⁴

¹ Faculty of Civil Engineering and Resource Management, AGH University Krakow, 30-059 Krakow, Poland; dworzak@agh.edu.pl (M.D.); michaltw@agh.edu.pl (M.T.); cala@agh.edu.pl (M.C.); jjakob@agh.edu.pl (J.J.); agnieszka.stopkowicz@agh.edu.pl (A.S.)

² Faculty of Natural Sciences and Mathematics, University of Banja Luka, 78000 Banja Luka, Bosnia and Herzegovina; suzana.gotovac.atlagic@unibl.org (S.G.A.); suncica.sukur@pmf.unibl.org (S.S.)

³ Conformity Assessment Body, Central Mining Institute—National Research Institute, 40-166 Katowice, Poland; mpytlik@gig.eu

⁴ Jerzy Haber Institute of Catalysis and Surface Chemistry, Polish Academy of Sciences, 30-239 Kraków, Poland; lukasz.kuterasiński@ikifp.edu.pl (Ł.K.); bogna.napruszewska@ikifp.edu.pl (B.D.N.)

⁵ Faculty of Physics and Applied Computer Sciences, AGH University Krakow, 30-059 Krakow, Poland; abaziak@student.agh.edu.pl

* Correspondence: abiess@agh.edu.pl; Tel.: +48-12-67-20-70

Abstract: The article presents the results of the third research stage on the potential microstructured charcoal additives in ANFO. The charcoal powder was liquid adsorption-treated with Fe in various ratios. Adding MC-Fe to ANFO changed the exothermic peak's position from ca. 280 °C to 250 °C due to lower activation energy, which influenced the kinetics of the reaction. Bruceton's test indicated that the MC-Fe addition to ANFO resulted in ca. 10% lower initiation energy in comparison with pure ANFO. However, the energy level did not influence the potential applicability of the additives. The fumes analysis indicated a lower concentration of CO for all tested samples; however, the concentration of NO_x rose. The thermodynamic calculations confirmed the experimental results, which could be explained by the increased positive oxygen balance. Moreover, all analyses showed that the most promising blasting properties referred to the ANFO sample containing the microstructured charcoal additive of a C:Fe ratio of 4:1. Therefore, further research will be dedicated to advanced studies between the chemical composition of this specific ANFO sample and its physicochemical and blasting properties.

Keywords: ANFO; microstructured charcoal; additives; blasting properties



Citation: Biessikirski, A.; Gotovac Atlagić, S.; Pytlik, M.; Kuterasiński, Ł.; Dworzak, M.; Twardosz, M.; Cała, M.; Jakóbczyk, J.; Sukur, S.; Stopkowicz, A.; et al. Influence of the Nano-Iron Oxide Adsorption-Enhanced Microstructured Charcoal Additives on the ANFO's Properties. *Energies* **2024**, *17*, 461. <https://doi.org/10.3390/en17020461>

Academic Editor: Manoj Khandelwal

Received: 28 December 2023

Revised: 12 January 2024

Accepted: 15 January 2024

Published: 17 January 2024



Copyright: © 2024 by the authors. Licensee MDPI, Basel, Switzerland. This article is an open access article distributed under the terms and conditions of the Creative Commons Attribution (CC BY) license (<https://creativecommons.org/licenses/by/4.0/>).

1. Introduction

Ammonium nitrate fuel oil (ANFO) is nowadays one of the most commonly used explosives in the mining industry and civil engineering [1]. From the chemical point of view, ANFO can be regarded as a combination of an oxygen component (ammonium nitrate(V)) with fuel oil (FO), which is characterized by a stoichiometric proportion of 94.5:5:5. According to results of previous research reported by Maranda et al. [2], Borowik et al. [3], and Biessikirski et al. [4], it was evidenced that ammonium nitrate(V) acting as an oxygen-bearing agent should be used in the form of porous prill (AN-PP).

ANFO is commonly applied as a mining and civil engineering explosive due to the relatively low cost of its manufacturing process and simplicity of production. Moreover, the vast possibility of adjusting ANFO's blasting properties by adding additives [5–7], adjusting the content between AN-PP and FO [8], or applying various types of FO [9–11]

is a significant advantage of ANFO. On the other hand, ANFO is classified as a non-ideal explosive material owing to significant differences between the measured values and predicted blasting properties. Miyake et al. highlighted that the non-ideal explosive behavior was evident in the area close to (and even below) the critical diameter. In that case, the detonation reaction could be supported due to the possible collapse of the progression of the detonation wave. Furthermore, it was evidenced that the velocity of detonation (VOD) was usually not able to reach its predicted values [12].

Apart from the most commonly used additives like aluminum, which strictly influences ANFO's blasting properties, better performance could be achieved by application of microstructured charcoal (MC) as an additive, since it was recently shown that, depending on the contents, it could have unique explosive combustion properties [13].

In the past, there were tests oriented to the possible application of coal powder. Xu et al. examined the reaction between ammonium nitrate(V) and coal [14]. They stated that inorganic carbon was almost nonreactive with ammonium nitrate(V), whereas the organic portion was highly reactive [14,15]. Furthermore, they concluded that the organic portion acted as a catalyst, which promoted the formation of nitric acid. HNO_3 subsequently oxidized the fuel [14,15]. Concerning the blasting properties of the prepared ANFO-based explosives, Miyake et al. tried to determine the detonation characteristic, VOD [16], and pressure peak [17] based on the steel tube tests. They studied ANFO with the addition of an activated carbon (AC). In turn, Nakamura et al. investigated ANFO blended with carbon powder [18]; meanwhile, Luri and Lianshen characterized in detail the thermal decomposition of ammonium powder under the influence of carbon black [19,20]. Except from our previous papers [21,22], there are no detailed tests reported about the possible application of MC for these purposes.

There, we examined the application of microstructured charcoal (MC) as a potential additive due to the MC's ability of high nitrogen adsorption capacity. We also conducted preliminary thermodynamic calculations and morphology analyses of the non-ideal explosive samples with the MC additives [21]. We found a high similarity between the calculated values and the properties measured experimentally. However, the results of the blasting tests reported in the paper [22] revealed differences between theoretical values and in situ tests. We observed that the best blasting properties were obtained in the case of the 1% addition of the MC powder of the grain size of 90 μm ; however, this was with almost triple emission of NO_x among post-blast fumes in comparison with the ANFO reference sample. The observed behavior of the tested MC-containing ANFO sample could be explained by an additional oxygen content in the MC chemical composition, which was proven by the XPS analysis. Another reason was a low BET surface. This was probably caused by the brittle structure, which resulted in clogging of the MC pores by fumes produced during pyrolysis [22]. In our recent paper, we eliminated the brittle structure by encrustation of the MC structure with Fe, which resulted in the change of the ANFO's blasting properties. Furthermore, we performed additional thermodynamic calculations with the *Explo5 v6.06.02* software based on the Becker–Kistiakowsky–Wilson (BKW) equation.

In this paper, we examined the non-ideal ANFO-based explosive, for which the chemical composition was defined as (AN-PP:FO:MC) 94.5:4.5:1.0 due to the most promising properties reported in [22].

2. Materials and Methods

2.1. Materials

AN-PP was manufactured by Yara's International A SA. AN-PP batch was produced in 2021. The bulk density was $0.82 \text{ g}\cdot\text{cm}^{-3}$ at 20°C . An average prill diameter was 1 mm. The detailed morphological description was presented in [21].

Microstructured charcoal (MC) in the form of powder was supplied by the HI Destilacija Teslić in Bosnia and Herzegovina. The MC powder was characterized by a grain size of $-90 \pm 0.0 \mu\text{m}$. The MC internal structure was incrustated with liquid adsorp-

tion treatment by Fe in the ratio of 3:1 (MC-Fe Sample 1), 4:1 (MC-Fe Sample 2), and 5:1 (MC-Fe Sample 3), Table 1. MC was produced and post-processed in 2022.

Table 1. General non-ideal explosive compositions, % wt.

| Sample Name | AN-PP, % wt. | FO, % wt. | MC, % wt. | C: Fe |
|-------------|--------------|-----------|-----------|-------|
| Sample 1 | 94.5 | 4.5 | 1.0 | 3:1 |
| Sample 2 | 94.5 | 4.5 | 1.0 | 4:1 |
| Sample 3 | 94.5 | 4.5 | 1.0 | 5:1 |

The fuel oil (FO) was produced in 2023 and was characterized by density and viscosity of $800 \text{ kg}\cdot\text{cm}^{-3}$ and $13.6 \text{ mm}^2\cdot\text{s}^{-1}$, respectively. The detailed physicochemical characteristics were provided in [9].

ANFO was produced by blending AN-PP with FO. The mixing process was performed at 250 rpm and it lasted for 20 min. MC-Fe powders were added at the end of the mixing process (5 min before the end of blending). ANFO with an MC additive was blended at 250 rpm for 5 min. The blending process was made in standard temperature ($20 \text{ }^\circ\text{C}$).

The chemical compositions of non-ideal explosive samples are presented in Table 1.

2.2. Methods

TG-DSC (Thermogravimetry—TG and Differential Scanning Calorimetry—DSC) of the ANFO with MC-Fe additives were conducted in the temperature range of $20\text{--}700 \text{ }^\circ\text{C}$. All investigated materials were exposed to an air atmosphere with flow of $30 \text{ mL}/\text{min}$. The airflow imitated the detonation conditions both in the furnace and the balance chamber. The temperature step was $5 \text{ }^\circ\text{C}\cdot\text{min}^{-1}$. The prepared sample (20 mg) was placed in the DSC aluminum pan directly before each experiment using a spatula. The TG baseline was determined using a heating profile for the empty pan. The TG drift was ca. $5 \text{ }\mu\text{g}$, which constituted $0.02 \text{ wt}\%$.

Theoretical blasting properties were calculated with Explo5 thermochemical computer code, developed by the OZM Research s.r.o. Thermodynamic calculations were established based on the Becker–Kistiakowsky–Wilson (BKW) equation. Based on the models, the detonation pressure, detonation temperature, and post-blast volume were established.

Fumes were measured according to the standard [23] that meets the EU Council directive [24]. Fumes analysis was conducted in the steel chamber. The chamber volume was 15 m^3 . The 14 g of RDX (Royal Detonation Explosives) primed the explosive charges with an electric instantaneous detonator. The non-ideal explosive mass was 600 g . An explosive was placed in the glass tube with a 46 mm diameter, Figure 1.



Figure 1. Exemplary non-ideal charge with a primer—Sample 1.

After the detonation, homogenized fumes were directed to the analyzers via the ventilation systems. An IR analyzer (MIR 25e) was used for the CO and CO_2 volume measurements. NO_x was determined by a chemiluminescent (TOPAZE 32M) analyzer. A detailed description of the research procedure was presented in [21].

The impact sensitivity test was performed in a Bruceton up-and-down test, according to [25]. The 35 mg loose granular powder sample was placed in the centre of the anvil

and the striker. The drop weight was elevated from a preselected height. The weight was dropped, and a noisemaker indicated the result. After the first reaction (called: “go”), successive drop heights were governed, and the drop height was adjusted. If the results were “go”, the drop height was lowered by one step. In the case of “no go”, the next height was one step higher. The energy was calculated based on Equation (1).

$$M = C + D \cdot [(A \cdot N^{-1}) \pm 0.5] \quad (1)$$

C is the logarithm of step height 0, D is the step interval in logarithm units, N is the total number of positive or negative reactions during the series, and A is the number of positive and negative reactions at each step. The standard deviation is calculated according to Equation (2).

$$S = 1.620 \cdot D \cdot [(N \cdot B \cdot A^{-1}) \cdot N^{-2} + 0.029] \quad (2)$$

where B is the number of positive and negative reactions at each step taken to the second power. The validity conditions shall be recorded between $0.5 \leq S \cdot D^{-1} \leq 2.0$.

Measurements of the heat of explosion values were performed in a detonation calorimeter. The tests were performed according to the methodology presented in [22].

2.3. Charcoale Enhancement with Iron Nanoparticles

The enhancement of micronized wooden charcoal was achieved by the co-precipitation of the two iron salts (FeCl_3 and FeSO_4) in order to form the iron oxide species with simultaneous adsorption on the charcoal surface. The selected ratios of carbon and total mass of Fe ions were C:Fe = 3:1, 4:1 and 5:1. The carbon samples (100 g each) were suspended in 200 mL of distilled water. The solution of iron salts was prepared by mixing iron chloride and iron sulphate in order to achieve the ratios mentioned above in relation to the carbon mass (33.33 g, 25 g, and 20 g of total mass of Fe ions). However, the mass ratio of iron Fe^{2+} to Fe^{3+} was kept at 4:1 for all three combinations. The solution was mixed on a magnetic stirrer for 30 min at 333 K (60 °C) and 200 rpm. The as-prepared solution was added in a carbon suspension and mixed on a magnetic stirrer for 40 min at 303 K (30 °C) and 200 rpm. This was followed by adding 2M NaOH solution drop by drop until a saturated alkaline pH of 14, and this is the period in which formation of the iron oxy-hydroxide species occurred with their simultaneous adsorption at the carbon surface. These mixtures were subjected to aging during 24 h at RT and filtered through white band filter paper. The drying of samples was performed in air atmosphere at 378 K (105 °C) and 423 K (150 °C) during 6 h and 2 h, respectively, where oxy-hydroxide species got transformed into nano-iron oxide forms.

3. Results and Discussion

The thermodynamic calculations of all non-ideal explosive compositions are given in Table 2.

Table 2. Theoretical properties of non-ideal explosives.

| Parameters | AN-PP:FO | AN-PP:FO:MC | Sample 1 | Sample 2 | Sample 3 |
|---|----------------|----------------|----------------|----------------|----------------|
| Enthalpy, $\text{kJ} \cdot \text{kg}^{-1}$ | −3885 | −4322 | −4330 | −4322 | −4322 |
| Detonation pressure, GPa | 3.630 | 3.912 | 3.604 | 3.615 | 3.620 |
| Detonation temperature, K (°C) | 2924 (2651) | 2883 (2610) | 2727 (2454) | 2780 (2507) | 2788 (2515) |
| Post-blast volume, $\text{dm}^3 \cdot \text{kg}^{-1}$ | 1032 | 1002 | 1044 | 1045 | 1045 |
| Density, $\text{kg} \cdot \text{m}^{-3}$ | 695 | 714 | 715 | 715 | 715 |
| VOD, $\text{m} \cdot \text{s}^{-1}$ | 4297 | 4388 | 4230 | 4256 | 4263 |
| Oxygen balance, % | −0.99 | 1.40 | 3.50 | 2.50 | 2.40 |

Table 2 shows the potential influence of MC-Fe on the non-ideal explosive properties. Based on the thermodynamic calculations, it can be stated that the incrustation of the MC with Fe by liquid adsorption treatment resulted in a change of the oxygen balance, which

should have a direct impact on the volume and the composition of the post-blast fumes. Particularly, an elevated C:Fe ratio should lead to a drop in the oxygen balance causing a lower volume of NO_x. The density of samples 1, 2, and 3 was close to the density of ANFO with the MC additive, which suggests the similar values of the velocity of detonation and heat of the explosion determined using theoretical calculations. In terms of non-ideal explosives, the VOD rises with an increased density until it reaches the dead pressed point. A relation between the VOD and density can be explained by an increased surface of contact between the fuel component and ammonium nitrate prill that stimulates the velocity of propagation of the chemical reaction zone, known as the velocity of detonation. In terms of ideal explosives, Cooper has indicated that the VOD is used to evaluate the detonation pressure and subsequently the explosive shock energy. Based on his equation, it is visible that the detonation pressure is directly proportional to the charge density and the VOD and inversely proportional to the specific heats of the detonation product gasses [26,27].

The calculation results showed that the addition of MC or MC-Fe to pure ANFO led to a decrease in the detonation enthalpy. Despite this fact, MC should combust behind the reaction front. Under normal conditions, when the inert component of a high standard enthalpy of formation is added to the explosive composition, the detonation temperature and pressure increase. In this scenario, the temperature rise appears until the additive component is completely burnt near the Chapman–Jouguet plain. A decrease in enthalpy will follow a further reduction in detonation temperature, and pressure that will result in a lower VOD.

The potential influence of the MC-Fe additive on the thermal decomposition of AN-PP is presented in Figures 2 and 3. The analysis was performed due to the possible interaction between Fe and the nitrous group, which resulted in oxidation during long-term storage at room temperature. The results of the thermal decomposition of pure AN and ANFO reported by Oxley et al. turned out to be helpful for us in the analysis of the obtained results in the TG-DSC studies. Oxley et al. observed four peaks: two endotherms at the beginning, one exotherm in the middle, and another endotherm at the end of the curve. The first endothermic peak occurred at 125 °C and the second at 169 °C. The melting point of AN-PP can explain these peaks. The exothermic peak had a maximum of 326 °C. It was about 100 °C wide. This peak can be defined as the primary decomposition exothermic reaction. A similar observation was reported by Babrauskas and Leggett [14], but no exothermic peak was found. It must be pointed out that there were detected only three endothermic signals, corresponding with the crystal phase transitions (peak not visible at 32 °C), the peak assigned to AN melting point at 169 °C, and the signal attributed to a primary decomposition reaction at 293 °C.

Regarding ANFO, Oxley et al. indicated that 5% content of fuel oil resulted in the appearance of the exothermic peak (ca. 292 °C) consisting of two submaxima at 256 °C and 287 °C. They concluded that 26% of the total released heat was related to the first exotherm. In turn, the addition of 1% MC powder of a grain size 90 µm to the ANFO caused a similar effect [28]. First, three endothermic peaks were observed. In the middle section, the exothermic peak was followed by the endothermic. The main exothermic peak was present at 282 °C [28]. The incrustation of the MC with Fe changed the position of the exothermic peak, Figure 2.

The DSC profiles depicted in Figure 2 indicated the presence of three endothermic peaks at 58, 134, and 174 °C, which was in line with the results reported in [15,28]. The exothermic peak at ca. 255 °C was found for all samples. In the case of the pure MC additive (1%, 90 µm grain size), the exothermic peak was located at ca. of 282 °C. The observed significant difference could be due to the interaction between Fe and the nitrous group. Iron could have a catalytic influence on AN decomposition, and during long-term storage, oxidation might have taken place. The parallel oxidation process lowered an activation energy that shifted the position of the exothermic peak. Moreover, the oxygen from the explosive's chemical composition will be primarily used for oxidation and further processes according to the Kistiakowsky–Wilson (K-W) rules. The lower activation energy

means that the energy needed to begin the process is lower than the activation energy of ANFO with the MC-Fe powder additive. At the end, the lower activation energy will impact the kinetics of the reaction (the reaction should take place faster and more volatile) and indirectly affect the heat of the explosion and fumes.

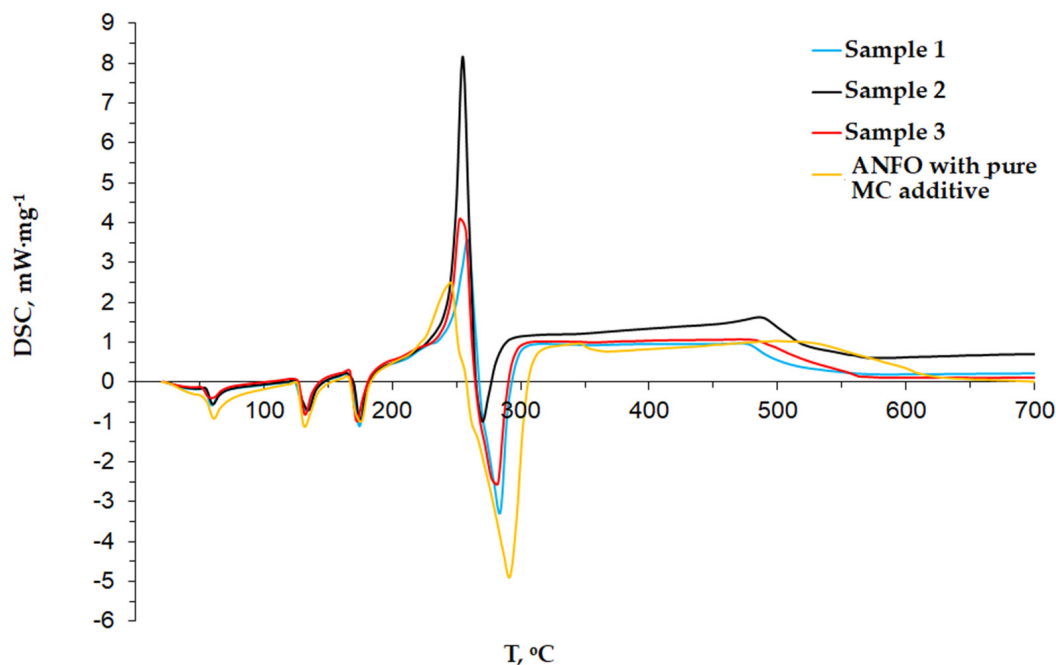


Figure 2. Results of DSC analysis.

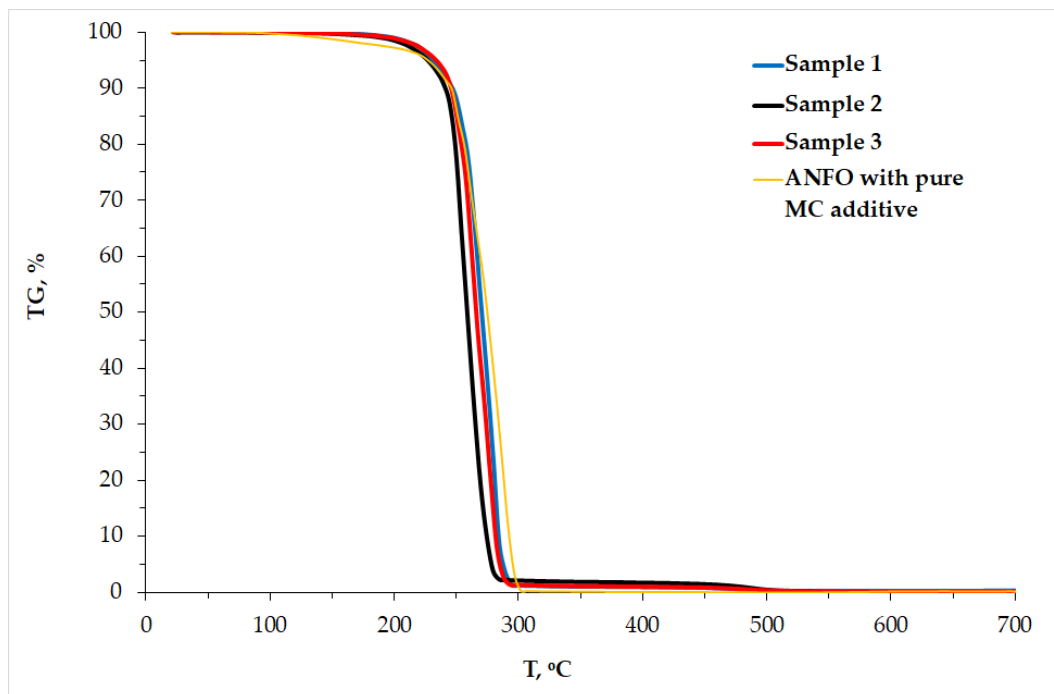


Figure 3. Results of TG analysis.

Moreover, the oxidation process and lower activation energy may affect the sensitivity of the explosives (impact energy). Furthermore, the DSC curve confirmed the results reported in [29] where heat flow increased very slowly and gradually in the range of temperature of ca. 190–232 °C and further rose sharply above 232 °C.

The exothermic peak was further followed by the endothermic maximum at ca. 269–284 °C range. This endothermic peak was not present in [14,28], but it was identified in our past studies [22,30,31]. This peak could be derived from the fuel component and the result of the bond breakages. This peak's intensity was evident for both the MC and the MC-Fe additions and confirmed that the fuel component influenced this endothermic peak.

The mass loss depicted in the TG curves (Figure 3) corresponded with the exothermic peaks visible in the DSC profiles. The 95% mass lost was found in the temperature range of 182–290 °C and took place as soon as the AN-PP melting point was reached. Our obtained mass loss characteristics turned out to be close to those in both our previous studies [22] and the results published in [15].

Due to the high ANFO impact sensitivity to the explosion, we determined the impact energy using the Bruceton machine. An exemplary result of ANFO under the Bruceton test was presented in Table 3.

Table 3. Bruceton tests results for ANFO, positive (“go”) approach.

| Height, cm | Number of Results: | | Iteration | Quantity | A | B |
|------------|--------------------|---------|-----------|----------|----|-----|
| | “go” | “no go” | | | | |
| 55 | 2 | 0 | 7 | 2 | 14 | 98 |
| 50 | 7 | 2 | 6 | 7 | 42 | 252 |
| 45 | 2 | 8 | 5 | 2 | 10 | 50 |
| 40 | 1 | 3 | 4 | 1 | 4 | 16 |
| 35 | 0 | 2 | 3 | 0 | 0 | 0 |
| 30 | 0 | 1 | 2 | 0 | 0 | 0 |
| 25 | 0 | 1 | 1 | 0 | 0 | 0 |
| 20 | 0 | 1 | 0 | 0 | 0 | 0 |
| Total | 12 | 18 | | 12 | 70 | 416 |

The impact energy was evaluated based on the total positive results of the tests. According to Equations (1) and (2), it was established that the ANFO standard deviation and impact energy were 4.9 and 49.58 J, respectively. The S/D was ca. of 1, confirming the validity conditions (it is assumed that only values in the range 1–2 were valid). The impact energy of ANFO with the MC-Fe additive was established at 46.67 J (Sample 1), 42.88 J (Sample 2), and 42.14 J (Sample 3). The calculated results confirmed the influence of Fe on the impact sensitivity of the non-ideal explosives. It can be observed that with a higher number of Fe atoms, the sensitivity increased. This means that a lower amount of energy is needed to initiate the explosive material. Furthermore, this follows the exothermic peak shift, which may indicate lower activation energy. However, to confirm this, a proper calculation based on, e.g., the Kissinger method, should be made. This observation is vital in terms of occupation and hazard. However, it should be noted that the difference between the indicative energy (49.58 J) and the energy of the non-ideal explosive with the MC-Fe additive was ca. of 10%. This means that, despite lower sensitivity, the non-ideal sensitive level is high enough and should not be treated as a threat.

The heat of the explosion was summarized in Table 4.

Table 4. The heat of the explosion of non-ideal explosives.

| Sample | MC or MC-Fe | Average Energy of Explosion, J·g ⁻¹ | Maximum Deflection, % |
|-----------|-------------|---|-----------------------|
| ANFO | - | 3940 | 0.5 |
| ANFO + MC | MC | 4100 | 0.3 |
| Sample 1 | 3:1 | 3972 | 0.3 |
| Sample 2 | 4:1 | 3988 | 0.2 |
| Sample 3 | 5:1 | 3980 | 0.3 |

Based on Table 4, it can be concluded that the MC-Fe additive slightly increased the average heat of the explosion (Sample 1–3, 3972–3988 J·g⁻¹) in comparison with pure

ANFO ($3940 \text{ J}\cdot\text{g}^{-1}$). However, it can be observed that the non-ideal explosives with the MC-Fe additives were characterized by lower heats of energy in comparison with ANFO with MC ($4100 \text{ J}\cdot\text{g}^{-1}$). The difference in the kinetics of the reaction could explain these discrepancies. A faster response should result in a lower activation energy. This observation confirmed the change in the position of the exothermic peak, Figure 2. The ANFO with the MC additive had greater activation energy due to the lack of the influence of Fe on AN-PP, which resulted in a lower reaction rate. In the case of samples 1–3, the reaction rates were faster due to the lower activation energy. Under normal conditions, it would probably finish with a higher detonation pressure and temperature; however, the parallel oxidation process, which appeared before the detonation phase, resulted in energy loss, and finally could result in a lower detonation temperature and pressure. In the Chapman–Jouguet (C-J) state, a close relation between pressure and energy was found. Namely, it can be stated that the reduction in pressure causes the energy drop. The small differences in energy between samples 1–3, namely: 3972 , 2988 , and $3980 \text{ J}\cdot\text{g}^{-1}$, respectively, could be explained by slight changes in their densities. According to the measurements, there were no visible differences between the sample densities; however, the different ratios of C:Fe should slightly influence it. Moreover, Sample 2 was characterized by the highest energy ($3988 \text{ J}\cdot\text{g}^{-1}$) among the non-ideal explosives with the MC-Fe additives, which was in line with the intensity of the exothermic DSC peak (Figure 2).

The result of the fumes analysis is presented in Table 5.

Table 5. In situ properties of the non-ideal explosives with the microstructure charcoal enhancer of $90 \mu\text{m}$ grain.

| Average Parameters | ANFO | ANFO with MC | ANFO with MC-Fe | | |
|--|--------|--------------|-----------------|----------|----------|
| | | | Sample 1 | Sample 2 | Sample 3 |
| Density, $\text{kg}\cdot\text{m}^{-3}$ | 693 | 691 | 691 | 691 | 691 |
| Volume of CO_2 , $\text{dm}^3\cdot\text{kg}^{-1}$ | 127.8 | 129.7 | 140.2 | 133.0 | 142.4 |
| The volume of CO, $\text{dm}^3\cdot\text{kg}^{-1}$ | 17.48 | 6.86 | 6.57 | 5.89 | 7.31 |
| Volume of NO, $\text{dm}^3\cdot\text{kg}^{-1}$ | 6.11 | 9.77 | 12.15 | 11.48 | 12.43 |
| Volume of NO_2 , $\text{dm}^3\cdot\text{kg}^{-1}$ | 0.49 | 0.85 | 0.84 | 1.01 | 1.45 |
| The volume of NO_x , $\text{dm}^3\cdot\text{kg}^{-1}$ | 6.60 | 10.62 | 12.99 | 12.49 | 13.88 |
| Total Volume of CO_x and NO_x post-blast fumes, $\text{dm}^3\cdot\text{kg}^{-1}$ | 158.50 | 157.91 | 172.76 | 164.92 | 177.46 |

The obtained concentrations of fumes indicated the non-ideal character of the tested explosives, which was particularly indicated by the total volume of the CO_x and NO_x gasses, which were in the range of 157 – $180 \text{ dm}^3\cdot\text{kg}^{-1}$. The received values can be explained by performing measurements close to the critical diameter of the studied charges. The temperature and pressure values obtained from the monitoring sensors indicated that the detonation was fully completed, and no inhibition effects were found during the whole procedure. A further increase in the charge diameter was not possible due to the limitation of the permissible charge for 1 m^3 of the blasting chamber and the borehole in the ballistic mortar. Therefore, the research presented in the current work has a preliminary character.

Based on the results from the post-blast fumes analysis summarized in Table 5, it can be concluded that the MC-Fe additives influenced fumes in all forms. The pure MC additive resulted in a similar total volume of fumes (ca. of $158.5 \text{ dm}^3\cdot\text{kg}^{-1}$) in comparison with ANFO (ca. of $158.5 \text{ dm}^3\cdot\text{kg}^{-1}$). The MC liquid adsorption-based incrustation with Fe led to the growth of the total volume of fumes (in the range of 165 – $177.5 \text{ dm}^3\cdot\text{kg}^{-1}$). It must be pointed out that the general oxide structure had also changed. It can be observed that ANFO with the MC-Fe additives resulted in an increase in the CO_2 and a decrease in CO in comparison with ANFO and ANFO with the pure MC additive. The rise in CO_2 can be explained by the oxidation of the CO according to K-W rules. Moreover, according to the thermodynamic calculations, the explosives with the MC-Fe additives were characterized by a positive oxygen balance between 2 and 3.5%, which had an impact on the production of NO_x within the post-blast fumes. The growth of the oxygen balance correlated clearly

with the volume of NO_x released during the detonation of explosives (Table 5). Based on the obtained results, it may be postulated that Sample 2 (with the C:Fe ratio of 4:1) was characterized by the lowest production of the post-blast fumes among all studied non-ideal explosives containing the MC-Fe additives. Our observations prompted us to conduct further research dedicated to the sample of the most promising properties (Sample 2). The planned research will focus on the reduction in NO_x production because of the detonation of the prepared explosive via the achievement of a zero-oxygen balance with a simultaneous limited influence on the energetic characterization of the studied non-ideal explosives.

4. Conclusions

Based on the results of the performed research, it may be concluded that the MC-Fe additives influenced the activation energy of the ANFO detonation. This statement was evidenced by the change in the position of the exothermic DSC peak from ca. 280 °C to 250 °C.

The presence of Fe reduced the AN decomposition temperature with a simultaneous acceleration of the AN decomposition rate, which was followed by the parallel oxidation process, resulting in a potential heat loss. In the C-J state, it also influenced both temperature and pressure, which should cause the lowering of the energy of the explosion in comparison with the non-ideal explosive with the MC.

From the analysis of the post-blast fumes, it may be postulated that the ANFO sample with a modifier of a C:Fe ratio of 4:1 was characterized by the least toxic chemical composition of the post-blast fumes among all studied ANFO explosives containing the MC-Fe additives. The CO content was smaller than for both pure ANFO and other counterparts containing the MC additives. However, the generation of the NO_x gasses was a result of the excess of oxygen in the material balance of the prepared ANFO samples. The experimental results were confirmed by the thermodynamic calculations. In future work, we are going to conduct the adjustment of AN-PP. We suspect that the drop in AN-PP granulation should shift the oxygen balance toward zero, which should lead to the reduced formation of NO_x among the post-blast fumes during the detonation of such prepared ANFO-based explosives.

The incrustation of Fe resulted in a decrease in sensitivity. The impact-sensitive tests indicated that the non-ideal explosives with the MC-Fe additives were characterized by an almost 10% lower impact energy. The lower initiation energy was essential concerning occupation and hazard. However, the energy level was high enough and should not lead to any uncontrolled decomposition reaction in terms of normal conditions of the explosive's application.

Author Contributions: Conceptualization, A.B. (Andrzej Biessikirski); methodology, A.B. (Andrzej Biessikirski), S.G.A., M.P., Ł.K. and B.D.N.; validation, A.B. (Andrzej Biessikirski), M.P. and M.D.; formal analysis, A.B. (Andrzej Biessikirski), S.G.A., Ł.K. and A.B. (Andrzej Baziak); investigation, S.G.A., A.B. (Andrzej Biessikirski), Ł.K., M.D., M.T., M.P., J.J. and B.D.N.; resources, A.B. (Andrzej Biessikirski), S.G.A. and S.S.; writing—original draft preparation, S.G.A., A.B. (Andrzej Biessikirski), Ł.K., M.D., M.T., M.P., A.S., M.C. and J.J. writing—review and editing, A.B. (Andrzej Biessikirski), J.J.; visualization, A.B. (Andrzej Biessikirski), S.G.A., Ł.K. and M.T.; supervision, A.B. (Andrzej Biessikirski). All authors have read and agreed to the published version of the manuscript.

Funding: The authors wish to thank for financial support for research no. 16.16.100.215 of The Faculty of Civil Engineering and Resource Management at the AGH University Krakow.

Data Availability Statement: The data presented in this study are available on request from the corresponding author Andrzej Biessikirski.

Conflicts of Interest: The authors wish to confirm that there are no known conflicts of interest associated with this publication, and there has been no significant financial support for this work that could have influenced its outcome.

References

1. Žganec, S.; Bohanek, V.; Dobrilović, M. Influence of a Primer on the Velocity of Detonation of ANFO and Heavy ANFO Blends Cent. Eur. J. Energetic Mater. **2016**, *13*, 694–704. [\[CrossRef\]](#)
2. Maranda, B.; Gołabek, J.; Kasperski, J. *Materiały Wybuchowe Emulsyjne*; Wydawnictwo Naukowo-Techniczne: Warszawa, Poland, 2015.
3. Borowik, M.; Biskupski, A.; Dawidowicz, M.; Buczkowski, D. Rules of Safe Storage of the Ammonium Nitrate Ferlitzers. *Przem. Chem.* **2013**, *92*, 2148–2152.
4. Biessikirski, A.; Kuterasiński, Ł.; Dworzak, M.; Pyra, J.; Twardosz, M. Comparison of structure, morphology and topography of fertiliser-based explosives applied in the mining industry. *Microchem. J.* **2019**, *144*, 39–44. [\[CrossRef\]](#)
5. Maranda, A.; Paszula, J.; Zawadzka-Małota, I.; Kuczyńska, B.; Witkowski, W.; Nikolczuk, K.; Wilk, Z. Aluminum powder influence on ANFO detonation parameters. *Cent. Eur. J. Energetic Mater.* **2011**, *8*, 279–292.
6. Fabin, M.; Jarosz, T. Improving ANFO: Effect of Additives and Ammonium Nitrate Morphology on Detonation Parameters. *Materials* **2021**, *14*, 5745. [\[CrossRef\]](#)
7. Zygmunt, B.; Buczkowski, D. Influence of Ammonium Nitrate Prills' Properties on Detonation Velocity of ANFO. *Propellants Explos. Pyrotech.* **2007**, *32*, 411–414. [\[CrossRef\]](#)
8. Onederra, I.; Bailey, V.; Cavanaugh, G.; Torrance, A. Understanding main causes of nitrogen oxide fumes in surface blasting. *Min. Technol.* **2012**, *121*, 151–159. [\[CrossRef\]](#)
9. Biessikirski, A.; Wądrzyk, M.; Janus, R.; Biegańska, J.; Jodłowski, G.; Kuterasiński, Ł. Study on fuel oils used in ammonium nitrate-based explosives. *Przem. Chem.* **2018**, *97*, 457–462.
10. Sinditskii, V.P.; Egorshv, V.Y.; Levshenkov, A.I.; Serushkin, V.V. Ammonium nitrate: Combustion mechanism and the role of additives. *Propellants Explos. Pyrotech.* **2005**, *30*, 269–280. [\[CrossRef\]](#)
11. Gunawan, R.; Zhang, D. Thermal stability and kinetics of decomposition of ammonium nitrate in the presence of pyrite. *J. Hazard. Mater.* **2009**, *165*, 751–758. [\[CrossRef\]](#) [\[PubMed\]](#)
12. Miyake, A.; Takahara, K.; Ogawa, T.; Ogata, Y.; Wada, Y.; Arai, H. Influence of physical properties of ammonium nitrate on the detonation behavior of ANFO. *J. Loss. Prev. Process Ind.* **2001**, *14*, 533–538. [\[CrossRef\]](#)
13. Choi, B.; Kim, C.; Yang, S.; Lee, S.; Kim, M.; Byun, S.; Jung, G.-G. Effective components on explosive combustion characteristics of wood charcoals. *Energy* **2020**, *197*, 117206. [\[CrossRef\]](#)
14. Xu, X.-X.; Wang, Q.; Zhu, Z.; Fu, X.-Q. Thermal stability of ammonium nitrate in high-temperature coal seam. *J. Therm. Anal. Calorim.* **2017**, *130*, 1171–1179. [\[CrossRef\]](#)
15. Babrauskas, V.; Laeggett, D. Thermal decomposition of ammonium nitrate. *Fire Mater.* **2020**, *44*, 250–268. [\[CrossRef\]](#)
16. Miyake, A.; Echigoya, H.; Kobayashi, H.; Katoh, K.; Kubota, S.; Wada, Y.; Ogata, Y.; Ogawa, T. Detonation velocity and pressure of ammonium nitrate and activated carbon mixtures. *Mater. Sci. Forum* **2008**, *566*, 107–112. [\[CrossRef\]](#)
17. Miyake, A.; Echigoya, H.; Kobayashi, H.; Ogawa, T.; Katoh, K.; Kubota, S.; Wada, Y.; Ogata, Y. Non-ideal detonation properties of ammonium nitrate and activated carbon mixtures. *Int. J. Mod. Phys. B* **2008**, *22*, 1319–1324. [\[CrossRef\]](#)
18. Nakamura, H.; Saeki, K.; Akiyoshi, M.; Takahashi, K. The reaction of ammonium nitrate with carbon powder. *Kayak. Gakkaishi J. Jpn. Explos. Soc.* **2002**, *63*, 87–93.
19. Lurie, B.A.; Lianshen, C. Kinetics and mechanism of thermal decomposition of ammonium nitrate powder under the action of carbon black. *Combust. Explos. Shock. Waves* **2000**, *36*, 607–617. [\[CrossRef\]](#)
20. Izato, Y.-I.; Miyake, A.; Echigoya, H. Influence of the physical properties of carbon on the thermal decomposition behavior of ammonium nitrate and carbon mixtures. *Sci. Technol. Energetic Mater.* **2009**, *70*, 101–104.
21. Atlagic, S.G.; Biessikirski, A.; Kuterasiński, Ł.; Dworzak, M.; Twardosz, M.; Sorogas, N.; Arvanitidis, J. On the Investigation of Microstructured Charcoal as an ANFO Blasting Enhancer. *Energies* **2020**, *13*, 4681. [\[CrossRef\]](#)
22. Biessikirski, A.; Gotovac Atlagić, S.; Pytlik, M.; Kuterasiński, Ł.; Dworzak, M.; Twardosz, M.; Nowak-Senderowska, D.; Napruszewska, B.D. The Influence of Microstructured Charcoal Additive on ANFO's Properties. *Energies* **2021**, *14*, 4354. [\[CrossRef\]](#)
23. EN 13631-16:2004; Explosives for Civil Uses. High Explosives. Part 16: Detection and Measurement of Toxic Gases. European Committee for Standardization: Brussels, Belgium, 2004.
24. European Union. Council directive 93/15/EEC of 5 April 1993 on the harmonisation of the provisions relating to the placing on the market and supervision of explosives for civil uses. *Off. J. Eur. Union* **1993**, *12*, 20–36.
25. STANAG 4489; Explosives, Impact, Sensitivity Tests. NATO: Brussels, Belgium, 1999.
26. Cooper, P.W. Acceleration, formation and flight of fragments. In *Explosives Engineering*, 1st ed.; Cooper, P.W., Ed.; Wiley-VCH: New York, NY, USA, 1996; pp. 385–394.
27. Kabwe, E. Velocity of detonation measurement and fragmentation analysis to evaluate blasting efficacy. *J. Rock Mech. Geotech. Eng.* **2018**, *10*, 523–533. [\[CrossRef\]](#)
28. Oxley, J.C.; Kaushik, S.M.; Gilson, N.S. Thermal decomposition of ammonium nitrate-based composites. *Thermochim. Acta* **1989**, *153*, 269–286. [\[CrossRef\]](#)
29. Sun, J.; Sun, Z.; Wang, Q.; Ding, H.; Wang, T.; Jiang, C. Catalytic effects of inorganic acids on the decomposition of ammonium nitrate. *J. Hazard. Mater.* **2005**, *127*, 204–210. [\[CrossRef\]](#)

30. Biessikirski, A.; Pytlik, M.; Kuterasiński, Ł.; Dworzak, M.; Twardosz, M.; Napruszewska, B.D. Influence of the Ammonium Nitrate(V) Porous Prill Assortments and Absorption Index on Ammonium Nitrate Fuel Oil Blasting Properties. *Energies* **2020**, *13*, 3763. [[CrossRef](#)]
31. Biessikirski, A.; Kuterasiński, Ł.; Dworzak, M.; Twardosz, M.; Tatko, M.; Napruszewska, B.D. On the Influence of the Ammonium Nitrate(V) Provenance on Its Usefulness for the Manufacture of ANFO Type Explosives. *Energies* **2020**, *13*, 4942. [[CrossRef](#)]

Disclaimer/Publisher's Note: The statements, opinions and data contained in all publications are solely those of the individual author(s) and contributor(s) and not of MDPI and/or the editor(s). MDPI and/or the editor(s) disclaim responsibility for any injury to people or property resulting from any ideas, methods, instructions or products referred to in the content.